CrossMark

# Microstructure and Mechanical Properties of Cast Al-5Zn-2Mg Alloy Subjected to Equal-Channel Angular Pressing

G.K. Manjunath ⓘ, G.V. Preetham Kumar, K. Udaya Bhat, and Prashant Huilgol

In the present work, cast Al-5Zn-2Mg alloy was processed through equal-channel angular pressing (ECAP) in route $B_C$ up to four number of passes. Microstructure and mechanical properties were investigated on processed and unprocessed materials. In cast condition, the material was composed of dendritic structure. After homogenization treatment, large-sized grains were observed. After ECAP processing, significant grain refinement was observed. After ECAP processing, high-density dislocations and high degree of misorientation between the grains were observed. In cast material, rod-shaped precipitates were observed, while, after ECAP processing, spherical-shaped precipitates were observed. ECAP processing leads to a noticeable improvement in the mechanical properties of the material. After four passes, 122% improvement in the microhardness and 135% improvement in the ultimate tensile strength of the material were observed. After three passes, a slight decrease in the mechanical properties was observed. This is attributed to the dissolution of the metastable $\eta'$ phase, annihilation of dislocations, dynamic recrystallization and texturing during ECAP processing. Brittle fracture mode was observed in tensile testing cast and homogenized samples. After ECAP processing, fracture mode was changed into shear fracture mode.

## 1. Introduction

Severe plastic deformation (SPD) techniques are the favoured techniques to develop ultra-fine-grained (UFG) materials (Ref 1). Among all SPD techniques, ECAP is a pioneer and efficient technique for the development of UFG materials (Ref 2). The procedure for ECAP processing was developed in 1981 by Segal and co-workers (Ref 3). Presently, numerous researchers have explored this technique on different metals and alloys. ECAP-processed materials exhibit high dislocation densities which lead to much higher hardness and strength than the materials processed by other conventional techniques (Ref 2). In ECAP processing, the deformation takes place by pure shear. The principle of ECAP is that a sample of uniform cross section (may be of circular or square cross section) is pushed through a set of channels having identical cross section, connecting at an angle (Φ). Large amount of shear strain is introduced in the material as it passes the plane of intersection between two channels, which in turn causes significant reduction in the grain size. The cross section of the material will be unaffected after processing, so the material could be processed repetitively, to accomplish large strain (Ref 4). Also, ECAP processing results in high degree of grain refinement along with the formation of high-angle grain boundaries. It is possible to develop required textures during ECAP by mod-

ifying the shear plane and direction of processing during a multiple pressing sequence. The ECAP processing can be easily scaled up for processing large-sized samples. ECAP processing is characterized by various parameters which describe the nature of the process. Major parameters in the ECAP processing are channel intersecting angle, processing routes, processing temperature and pressing speed. These parameters play a vital role in determining the nature of the grain structure developed through ECAP (Ref 2).

The Al-Zn-Mg alloys are identified as the hardest and strongest alloys among the aluminum alloy families (Ref 5). The Al-Zn-Mg alloys have an extensive application in the development of lightweight structures such as road tankers, transportable bridge girders, military vehicles and railway wagons. The Al-Zn-Mg alloys are also increasingly being used to manufacture hulls of ships (Ref 6). Numerous researches were stated to examine the importance of ECAP processing on 7000 series aluminum alloys. But, very few researches were reported to examine the importance of SPD and other metal forming process on the cast alloys composed of only aluminum, zinc and magnesium. Gopala Krishna et al. (Ref 7) reported the tensile characteristics of UFG Al-4Zn-2Mg alloy developed by cryorolling and reported that concurrent enhancement in strength and ductility is due to the combination of cryorolling and heat treatment. Mazilkin et al. (Ref 8) studied the structure and composition of the cast Al-5Zn-2Mg and Al-10Zn-4Mg alloy subjected to high-pressure torsion (HPT). Kogtenkova et al. (Ref 9) studied the phase transformations during HPT of cast Al-5Zn-2Mg and Al-10Zn-4Mg alloys. Mazilkin et al. (Ref 10) studied the hardness of nanostructured cast Al-5Zn-2Mg and Al-10Zn-4Mg alloys subjected to HPT. Gopala Krishna et al. (Ref 11) studied the microstructural development and aging behavior of Al-4Zn-2Mg alloy subjected to cryorolling. Yang et al. (Ref 12) reported the fatigue properties and features of fatigue-fractured Al-5Zn-2Mg alloy which was subjected to rolling process.

**G.K. Manjunath, G.V. Preetham Kumar, K. Udaya Bhat,** and **Prashant Huilgol**, Department of Metallurgical and Materials Engineering, National Institute of Technology Karnataka, Surathkal, Mangalore 575025, India. Contact e-mail: manjugk2001@gmail.com.

Generally, in wrought 7000 series aluminum alloys, along with zinc and magnesium, other elements (Cu and Zr) are present, which leads to the development of different sets of precipitates (like $Al_2Cu$, $Al_3Zr$). It is difficult to identify the effect of each precipitate on the strength of the alloy. But in the present study an alloy composed of only aluminum, zinc and magnesium was selected. In this combination, only $MgZn_2$ precipitate formation takes place, which is a hexagonal close-packed (HCP) structure and helps in increasing the strength of the alloy. From this alloy combination, strengthening contribution from other precipitates is eliminated which are present in wrought 7000 series aluminum alloys. The present study was inspired by the realization that in previous studies no efforts were made to study a cast alloy composed of only aluminum, zinc and magnesium and processed through ECAP technique. The present study is aimed to process cast Al-5Zn-2Mg alloy through ECAP technique and to investigate its effect on microstructure and mechanical properties. This alloy is presently used in the fabrication of lightweight structures of aerospace and automobile equipments (Ref 7). After ECAP processing, improvement in the strength and ductility of the material was observed, which is a required property of engineering materials. Mainly, this type of observations was rarely identified in the ECAP-processed samples. Also, the morphology of the precipitates present in the cast material is deeply discussed using TEM analysis and the effect of ECAP processing on the change in morphology and fragmentation of the precipitates is deeply discussed using TEM analysis.

## 2. Materials and Methods

### 2.1 Material Preparation

The alloy studied in the present work was prepared by gravity casting method. Melting was carried out in an electric resistance furnace with automatic temperature controller. At first, silicon carbide crucible was placed inside the furnace, and then, the furnace was heated to 50 °C above the melting temperature of the alloy. Once the required temperature was achieved, commercial pure aluminum (99.7%) pieces of required quantity were charged into the crucible. Once the aluminum charge was melted, pure zinc (99.9%) granules and pure magnesium (99.9%) granules packed in the aluminum foils were added to the melt and stirred using a graphite rod. Later, the melt was degassed with hexachloroethylene tablets. To avoid the surface oxidation effect, covering flux was applied on the melt and the dross present on the surface was removed. Later, the melt was poured into a steel die which is preheated to 400 °C. In order to achieve homogenous composition, the solidified alloy was remelted again. Firstly, the alloy was cast into circular bars of Ø 25 and 100 mm long. The composition of the material was verified through optical emission spectroscopy (OES) technique. Table 1 presents the composition of the material verified through OES technique. After casting,

homogenization of the cast alloy was carried out at 480 °C for 20 h. For ECAP processing, homogenized materials were machined to Ø 16 and 85 mm long.

### 2.2 ECAP Processing

Figure 1 shows the three-dimensional exploded view of the ECAP die assembly used in the present work. The ECAP die was machined from H11 tool steel followed by heat treatment to attain 50 HRc hardness. The ECAP die was fabricated in split-type design (two-piece die), and align pins were provided for proper alignment. The ECAP die was machined with two channels of 16 mm diameter intersecting at an angle (Φ) of 120° and outer arc curvature (Ψ) of 30°. The magnitude of the strain imposed on the sample with these angular values in each pass is evaluated by analytical approach, and the strain value evaluated is based on the assumption that no friction effect is present between the die and the sample. The assumption becomes more realistic under the condition of application of proper lubrication. Iwahashi et al. (Ref 13) have given the expression for the equivalent strain ($\varepsilon_N$) considering $N$ number of passes as

$$\varepsilon_N = \frac{N}{\sqrt{3}}\left[2\cot\left(\frac{\phi}{2}+\frac{\psi}{2}\right) + \psi\mathrm{cosec}\left(\frac{\phi}{2}+\frac{\psi}{2}\right)\right]. \qquad \text{(Eq 1)}$$

The strain imposed on the sample with these angular values in each pass is 0.667. The 'Ψ' angle has relatively less effect on the strain imposed on the sample when the angle 'Φ' is more than 90°. To impose high strain, it is desirable to construct a die with very low values of 'Φ' and 'ψ.' In the present work, route $B_C$ was adopted. It results in uniform distribution of the strain in the material compared with other routes. Also, route $B_C$ provides optimum processing condition for attaining a homogeneous microstructure of equiaxed grains separated by high-angle grain boundaries and hence isotropic mechanical properties are expected. Also, processing through route $B_C$ gives shearing over larger angular ranges in comparison with other processing routes (Ref 14). Samples were attempted to process at lowest possible temperature in route $B_C$ up to four number of passes. ECAP processing was carried out in a universal testing machine at a speed approximately equal to 0.5 mm per second. Molybdenum disulfide ($MoS_2$) paste was used as lubricant to reduce friction effect between the die and specimen. Before processing, the ECAP die is heated to required temperature using heating coils. Once the required temperature was attained, the sample was placed inside the die and retained for 15 min so the temperature evenness was attained between the die and sample. During processing, die setup was maintained at the required processing temperature.

### 2.3 Material Characterization

Following ECAP, microstructural analysis was carried out on both unprocessed and processed materials. Microstructural study was conducted by using ZEISS AX10 LAB A1 optical microscopy (OM) and JEOL JSM 6380LA scanning electron

**Table 1 Chemical composition (in wt.%) of the alloy, verified through OES**

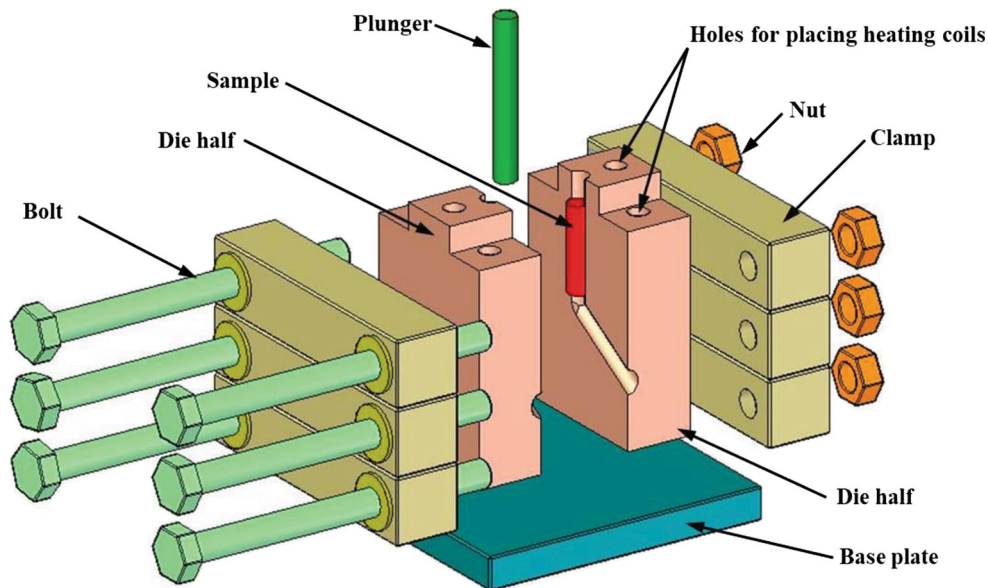| Element | Al | Zn | Mg | Fe | Si | Mn | Cu | Zr | Ni | Ti | Pb | Cr |
|---|---|---|---|---|---|---|---|---|---|---|---|---|
| wt.% | 92.4 | 5.09 | 2.07 | 0.21 | 0.13 | 0.072 | 0.019 | 0.003 | 0.001 | 0.002 | 0.001 | 0.002 |

**Fig. 1** Three-dimensional exploded view of the ECAP die assembly used in the present study

microscopy (SEM). For microstructure analysis, unprocessed and processed specimens were sectioned perpendicular to the processing direction. Specimens were prepared by metallographic techniques and etched with Keller's etchant. Grain size measurements before and after ECAP processing were taken by linear interception method using ImageJ software.

To identify the grains and morphology of the precipitates present in the samples, JEOL JEM-2100 transmission electron microscopy (TEM) operating at 200 kV was used. Both unprocessed and processed samples were thinned down to 80 μm thickness, and the disks of Ø 3 mm were pierced from the thinned samples. The punched disk is further thinned down to 40 μm thickness by disk polishing. The samples were then dimpled to 20 μm thickness using dimple grinder. Ion milling of the dimpled sample was carried out at 4° beam angle with beam energy of 4 keV till perforation was attained. The ion-milled samples were studied under TEM and selected area electron diffraction (SAED) patterns were collected. TEM equipped with energy-dispersive spectroscopy (EDS) facility was used to analyze the chemical composition. JEOL x-ray diffractometer (XRD) was used to study the phases developing in the material. The XRD analysis was conducted with a speed of 1° per min using Cu-Kα radiation at 20 mA current and 30 kV tube voltage.

### 2.4 Material Testing

Hardness was measured by using Shimadzu Vickers hardness tester (model: HMV-G20 ST). The Vickers microhardness, Hv, was determined by imposing a load of 50 g for 15 s. Hardness was measured perpendicular to ingot axis in cast and homogenized samples, and in ECAP-processed samples, hardness was measured perpendicular to the processing direction. To achieve optimal results in the hardness measurement, center portion of the material was selected in both unprocessed and processed materials. On each sample, ten hardness measurements were taken and average values were considered. Tensile tests were carried out to estimate the ultimate tensile strength

(UTS) and elongation to failure (ductility) of the unprocessed and processed specimens. Tensile tests were conducted at room temperature and at a constant cross-head movement of 0.1 mm/min by using Shimadzu universal testing equipment (model: AG-X plus™ 100 kN). For tensile testing, unprocessed and processed samples were machined to tensile test samples as per the ASTM E8 standard. Figure 2 shows the schematic diagram of the tensile test specimen with dimensions. In each condition, three samples were tested to check the repeatability of the results and average values were considered. The fracture modes of the tensile test specimens were identified macroscopically (visual appearance), and fracture surface morphology of the tensile test specimens was analyzed by using SEM.

## 3. Results and Discussion

The alloy was successfully processed at 150 °C up to four number of passes. This was the lowest temperature at which the samples would be successfully ECAP processed in route $B_C$ without cracking. Figure 3 shows the macroviews of the samples which were cracked during ECAP processing at temperature less than 150 °C. It was also observed that the intensity of the crack reduces with an increase in the processing temperature. Figure 4 shows the macroviews of the samples processed at 150 °C up to four number of passes in route $B_C$ without cracking.

### 3.1 Microstructure Evolution

**3.1.1 Optical Microscopy.** Figure 5 presents the OM images of the material in various conditions. In cast condition, the material is composed of dendritic morphology as shown in Fig. 5(a). After homogenization treatment, grain boundaries were observed as shown in Fig. 5(b). Significant grain refinement was observed after ECAP processing. After the first and second passes, sub-grains were perceived inside the
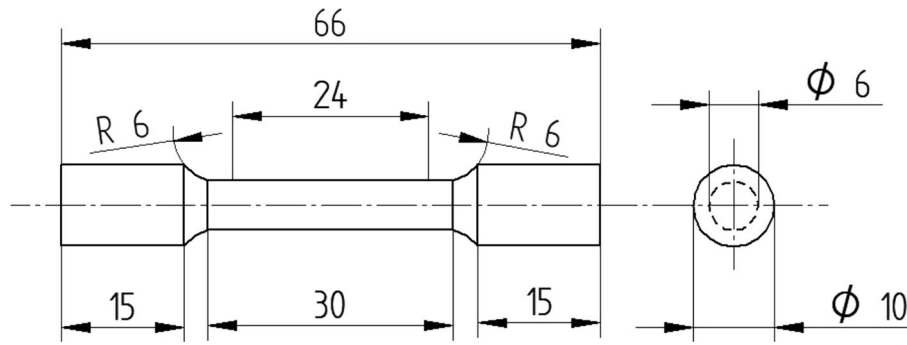
**Fig. 2** Schematic diagram of the tensile test specimen (Note: All dimensions are in mm)
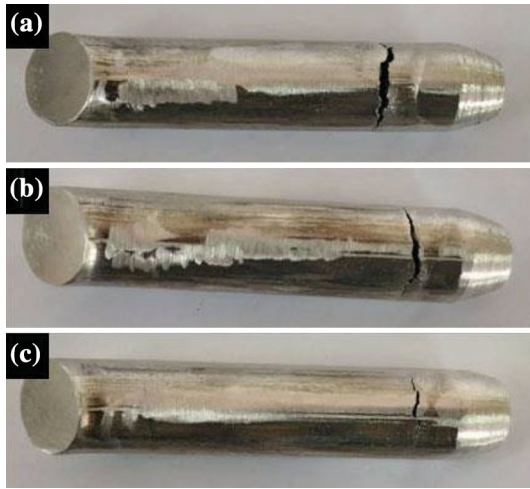


**Fig. 3** Al-5Zn-2Mg alloy ECAP processed (a) first pass at room temperature, (b) first pass at 100 °C and (c) first pass at 125 °C, respectively



**Fig. 4** Al-5Zn-2Mg alloy ECAP processed up to four number of passes at 150 °C

grains and also small numbers of elongated grains were observed, as shown in Fig. 5(c) and (d). Grain refinement rate is high during the first and second passes during ECAP processing, due to a large rate of dislocation generation. After the third and fourth passes, the large number of macro- and microtwinning in grains was observed, as displayed in Fig. 5(e) and (f). Twinning direction is nearly parallel to the processing direction. It is noted that in route $B_C$ deformation restores the equiaxed structure in each plane after every four consecutive passes and deformation occurs in all three planes (Ref 15).

**3.1.2 Scanning Electron Microscopy.** The SEM micrographs of the material in various conditions are presented in Fig. 6. Microstructure of the material in cast condition is presented in Fig. 6(a). In this condition, the microstructure was compiled of dendrites of size $200 \pm 20$ μm. Microstructural study of the material in this condition confirmed the existence of dendrites with precipitates in the α-Al matrix (Ref 16). Precipitates in α-Al matrix were identified as $\eta'$ (MgZn$_2$) precipitates (Ref 17). Figure 6(b) presents the SEM micrograph of the material in homogenized condition. At this stage, grain boundaries were clearly visible due to recrystallization and grain growth happened during homogenization. After homogenization, grains of size $180 \pm 20$ μm were observed. During homogenization treatment, precipitates located in the inter-dendritic regions were uniformly dissolved in the aluminum. It was observed that ECAP processing leads to a considerable decrease in the grain size. After the first pass, array of sub-grains was introduced within the grains and the precipitates growth was observed near the grain boundaries. These precipitates were renowned as GP zones and $\eta'$ (MgZn$_2$)-phase precipitates (Ref 18). After the first pass, sub-grains of $25 \pm 8$ μm in size were perceived as shown in Fig. 6(c). After the second pass, more volume fraction of sub-grains was developed inside the grains as shown in Fig. 6(d). At this stage, sub-grains size was reduced to $15 \pm 5$ μm. After the third pass, shear bands were identified inside the grains and sub-grains as shown in Fig. 5(e). At this stage, shear bands of $6 \pm 3$ μm in size were observed. After the fourth pass, a large number of shear bands were observed as shown in Fig. 6(f). The size of the shear bands measured at this stage is $3 \pm 2$ μm. Homogeneous and equiaxed microstructure was perceived in the third and fourth passes because the dynamic recrystallization occurred during ECAP at 150 °C and static recrystallization occurred during initial heating of the material.

**3.1.3 Transmission Electron Microscopy.** Figure 7 presents the TEM micrographs and associated SAED patterns of the material in different conditions. Figure 7(a) presents the TEM
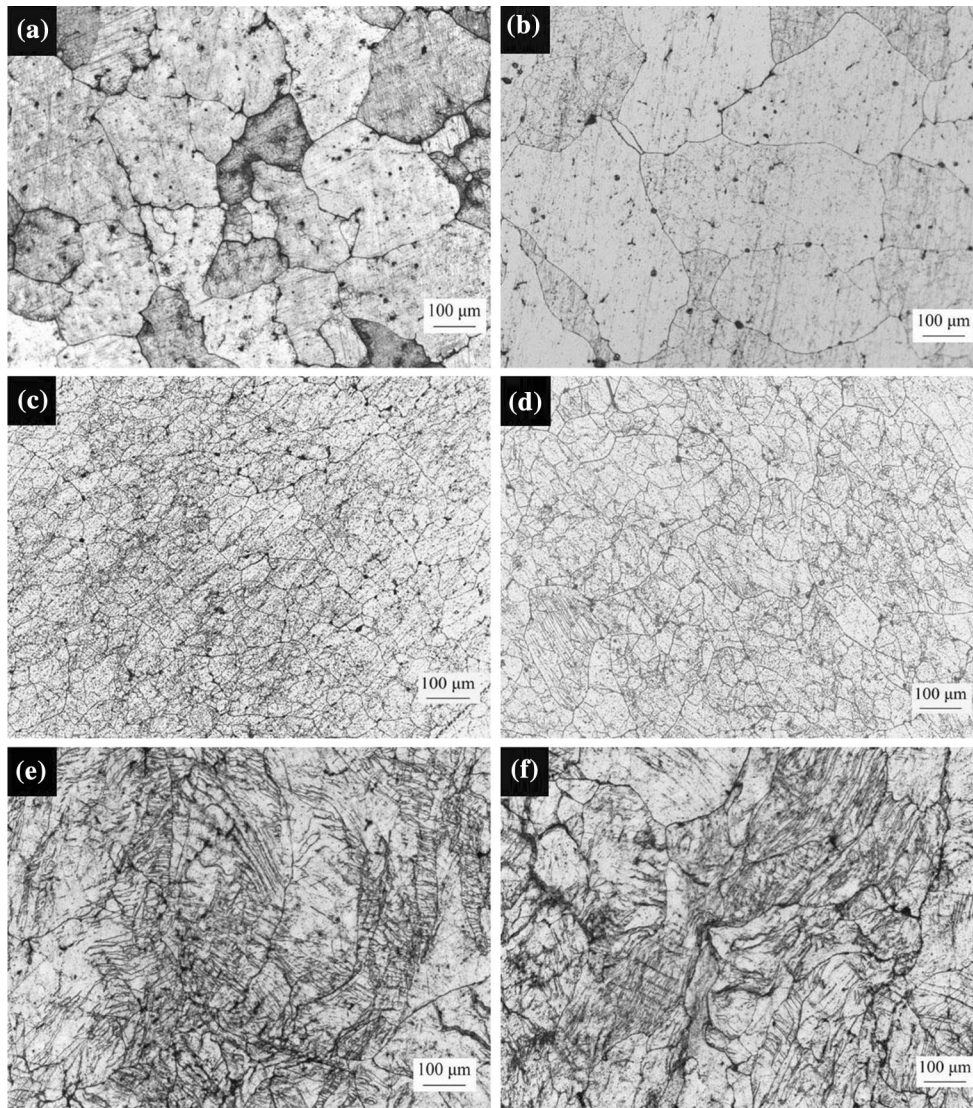
**Fig. 5** OM images of the alloy (a) cast, (b) homogenized, (c) first pass, (d) second pass, (e) third pass and (f) fourth pass

micrograph of the material in cast condition. In this condition, dendritic structure with low-density dislocations was observed and SAED pattern in the cast condition confirms the presence of low angle of misorientation between the dendrites. Also, precipitates were lying near the dendrites and in the inter-dendritic regions. Figure 7(b) presents the TEM micrograph of the material in homogenized condition. In this condition, an array of grains with low-density dislocations was observed. Also, SAED pattern in the homogenized condition confirms the presence of low angle of misorientation between the grains. TEM micrograph of the material after the first pass is shown in Fig. 7(c). It indicates that grain size has significantly decreased. The microstructure after the first pass consists of deformation bands (shear bands) with increased dislocation density. These deformation bands were formed due to elongation of the grains. The grains were literally elongated in the processing direction, and width of the elongated grains was approximately 800 nm. SAED pattern confirms the existence of low angle of misorientation between the grains. The presence of low angle of misorientation between the grains is in consistent with previous ECAP studies on pure aluminum after the first pass (Ref 19).

Figure 7(d) shows the TEM micrograph of the material after the second pass. At this stage, deformation bands which are developed in the first pass are sliced by the deformation bands developed in the second pass. Considerable increase in disloca-tion density was observed compared with the first pass. The presence of distinct dots in the SAED pattern confirms the existence of some fraction of low angle of misorientation between the grains. TEM micrograph of the material after third pass is displayed in Fig. 7(e). At this stage, an increase in the dislocation density was perceived compared with previous passes. The SAED pattern after the third pass confirms the formation of the grains with high angle of misorientation, although presence of low angle of misorientation between the grains was also observed. TEM micrograph of the material after the fourth pass is displayed in Fig. 7(f). At this stage, equiaxed grain structure has replaced the band-like structure formed in the first pass. High density of dislocations was observed. The SAED pattern after the fourth pass confirms the existence of large volume of high angle of misorientation between the grains.

Figure 8 presents the morphology and distribution of precipitates of the material in different conditions. Figure 8(a)
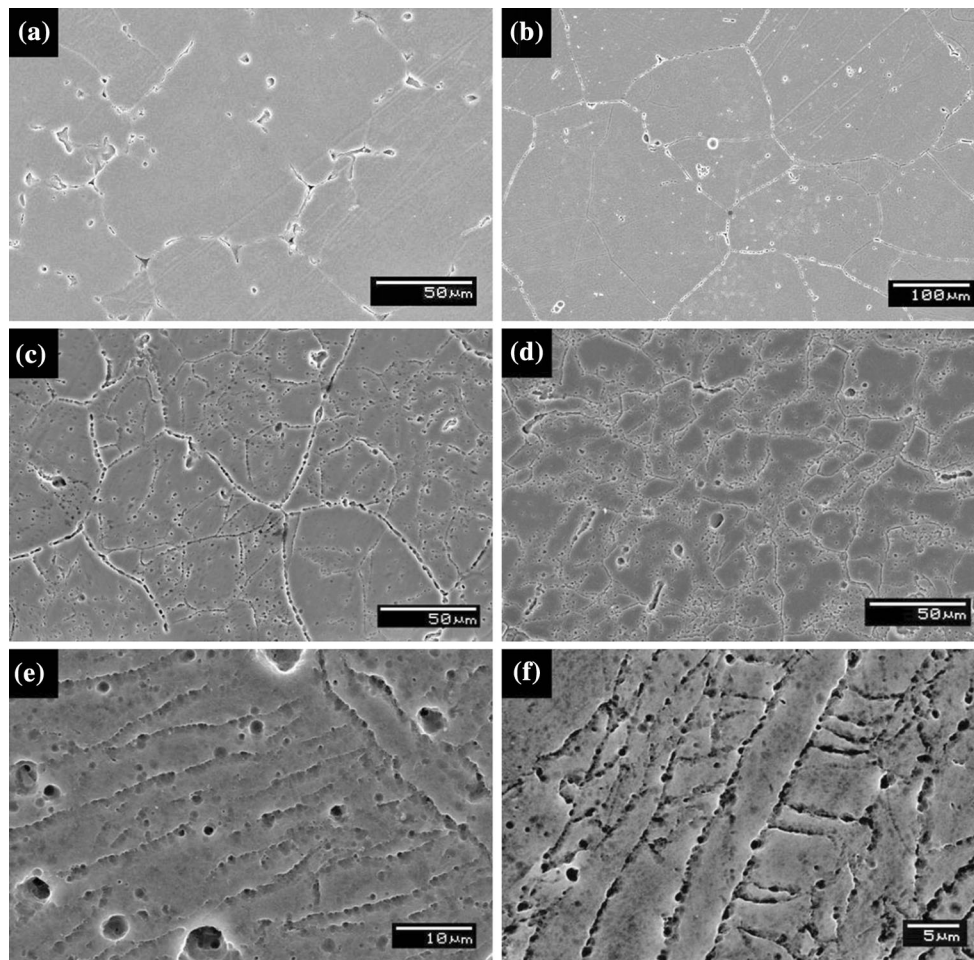
**Fig. 6** SEM micrographs of the alloy (a) cast, (b) homogenized, (c) first pass, (d) second pass, (e) third pass and (f) fourth pass

shows the morphology of the precipitates present in the cast condition. In this condition, high density of rod-shaped $\eta'$ (MgZn$_2$) precipitates was observed. The presence of rod-shaped $\eta'$ (MgZn$_2$) precipitates in cast condition is in consistent with earlier observations in Al-11.5Zn-2.5Mg cast alloy (Ref 20). The average length and width of the rod-like precipitates were measured as approximately 150 and 25 nm, respectively. Figure 8(b) presents the morphology of the precipitates present in the alloy after the first pass. There was a noticeable change in the shape of the precipitates compared with cast condition. After the first pass, spherical-shaped precipitates in the size range of 20 to 40 nm were observed. Also, there is substantial fragmentation of the precipitates. The precipitates were identified as $\eta'$-phase (intermediate metastable) precipitates (Ref 21). Figure 8(c) presents the morphology of the precipitates existing in the alloy after the fourth pass. The morphology of the precipitates was not changed with an increase in the number of passes and fragmentation of precipitates continued in the fourth pass. The size of the precipitates was decreased to approximately 10 to 20 nm. The decrease in the size of the precipitates is due to shearing of the precipitates by the dislocations introduced in the subsequent passes. These precipitates were identified as stable $\eta$ (MgZn$_2$)-phase precipitates (Ref 22). Figure 9 shows the EDS examination of the alloy in cast condition and after four ECAP passes. The EDS exami-

nation was carried out on both the matrix and the precipitates. It is confirmed from the EDS examination that the matrix is composed of aluminum and precipitates present in the alloy are composed of zinc and magnesium.

### 3.2 XRD Analysis

Formation of precipitates in Al-Zn-Mg alloys will be in the order starting with solid solution (SS) to Guinier–Preston zones (GP zones) $\rightarrow \eta' \rightarrow \eta$ (Ref 23). Normally, GP zones will be formed in Al-Zn-Mg alloys over the temperature ranging from ambient to 120 °C (Ref 24). ECAP processing accelerates the precipitation kinetics, and the precipitation kinetics is also accelerated when the processing temperature is increased (Ref 25). The reason for accelerating in the precipitation kinetics is owing to the formation of additional nucleation sites during ECAP processing and also owing to the increase in the diffusion rate due to increased temperature (Ref 25). Results of XRD analyses of the cast, homogenized and ECAP-processed samples are presented in Fig. 10. In cast condition, along with aluminum peaks, other peaks are also perceived. Peaks at $2\theta = 20°$ are from the GP zones and peaks at 40° to 50° are from the metastable $\eta'$ phase (Ref 23). In homogenized material, reflections for GP zones and $\eta'$ phase were not observed and only aluminum reflections were observed. In the
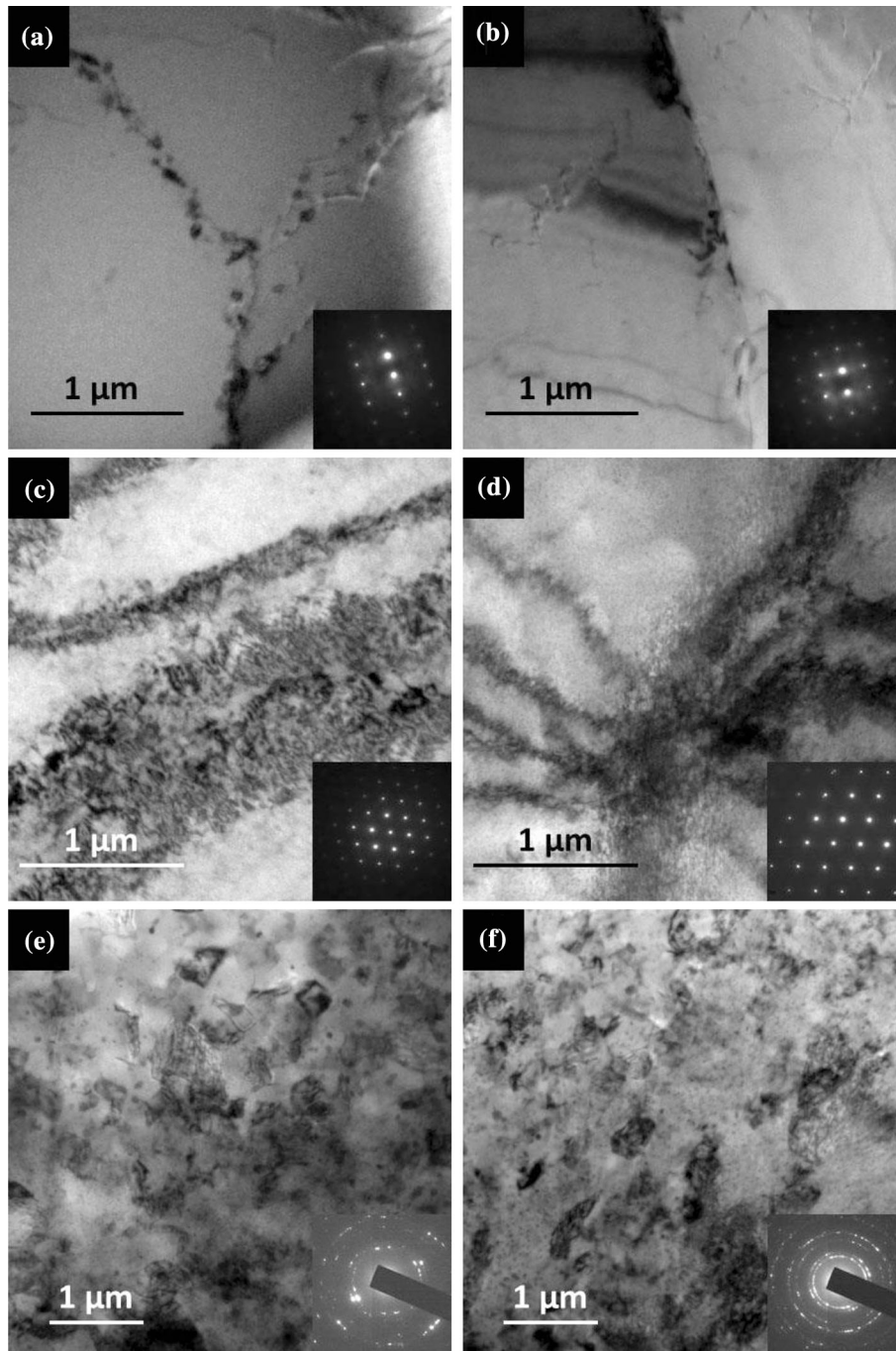
**Fig. 7** TEM micrographs and associated SAED patterns (a) Cast, (b) Homogenized, (c) first pass, (d) second pass, (e) third pass and (f) fourth pass

homogenization process, precipitates located near the interdendritic regions were dissolved in the aluminum. This is in consistent with SEM and TEM observations on the homogenized material. After the first pass, dislocations were introduced in the material and these dislocations act as nucleation sites for nucleation of $\eta'$ phase and GP zones (Ref 18). Therefore, after the first pass, along with aluminum peaks, other peaks were also observed. This is in consistent with SEM and TEM observations after the first pass. It was observed that when the number of passes increased, $\eta'$ peaks slowly changed into $\eta$ peaks, signifying $\eta'$ phase changed into $\eta$ phase (Ref 22). The

$\eta'$ phase precipitates were sheared into small particles by dislocations moving along (111) planes (Ref 24).

### 3.3 Mechanical Properties

**3.3.1 Hardness.** Figure 11 indicates the changes in the microhardness of the material under various conditions. In cast condition, the microhardness of the alloy is $90 \pm 8$ Hv. After homogenization, the microhardness was enhanced to $105 \pm 6$ Hv. After ECAP processing, significant enhancement in the microhardness of the material was perceived. The
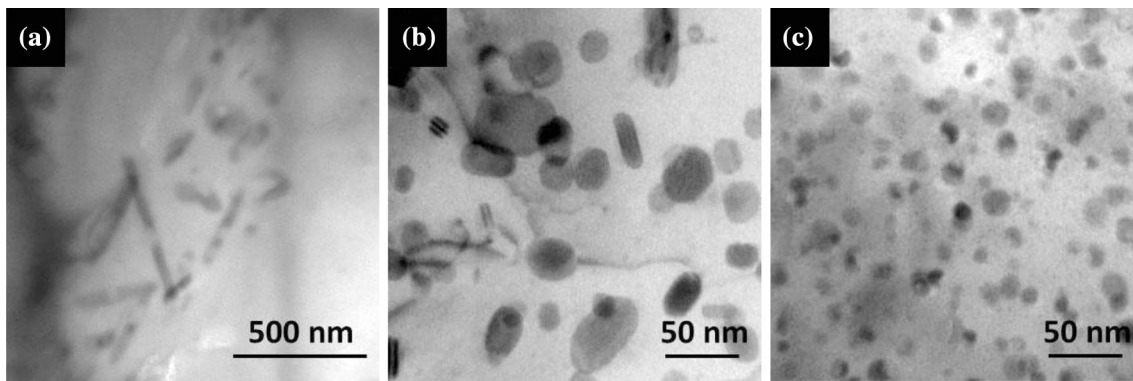
**Fig. 8** TEM micrographs showing the morphology and distribution of precipitates (a) Cast, (b) first pass and (c) fourth pass
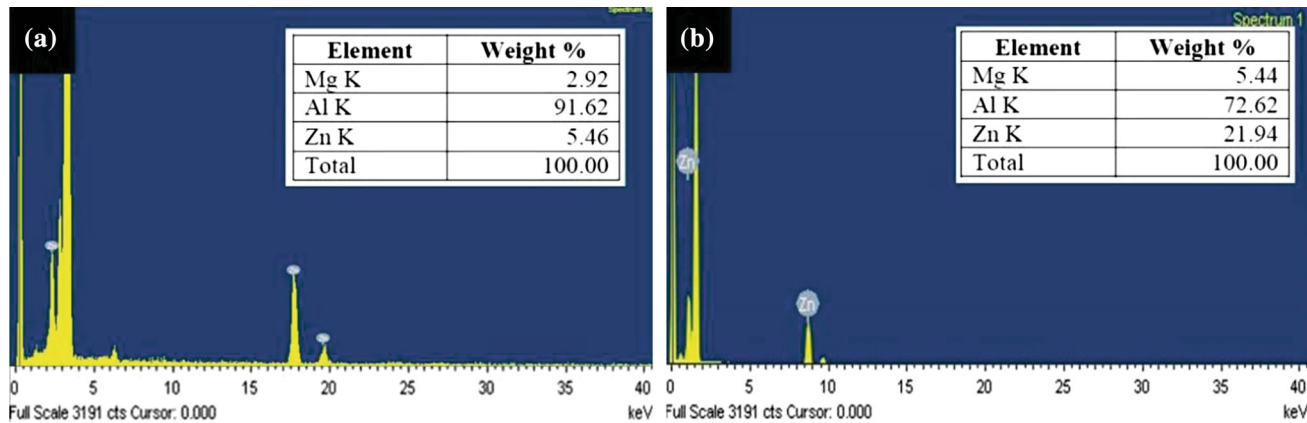


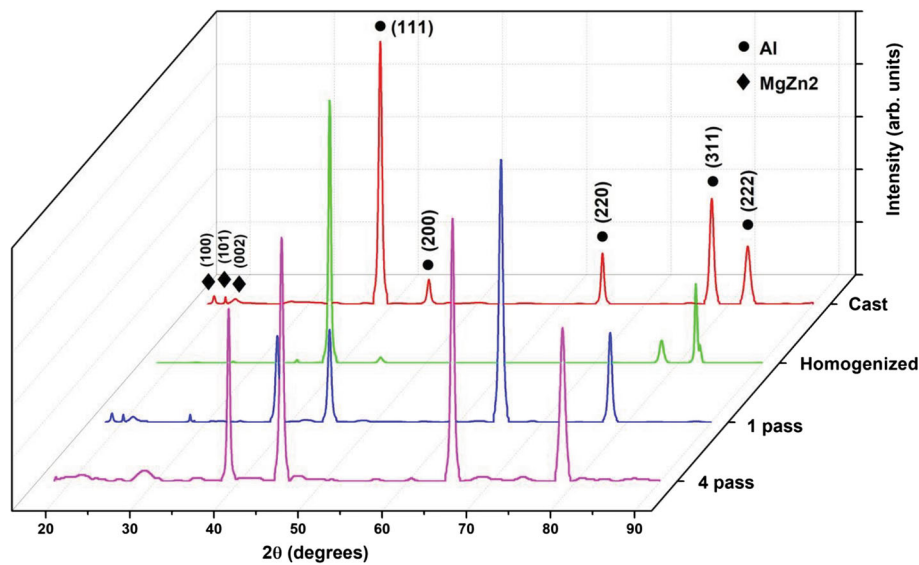**Fig. 9** EDS analysis in TEM (a) cast and (b) fourth pass



**Fig. 10** XRD patterns of the alloy in different conditions

microhardness of the alloy was enhanced to $168 \pm 6$ and $192 \pm 5$ Hv in the first and second passes, respectively. But the microhardness was reduced to $188 \pm 4$ Hv after the third pass, and it again increased to $200 \pm 4$ Hv in the fourth pass.

Microhardness was enhanced by 17% after homogenization treatment. After the first and second passes, the microhardness was enhanced by 87 and 113%, respectively, from the initial condition. Even though the microhardness of the alloy after the
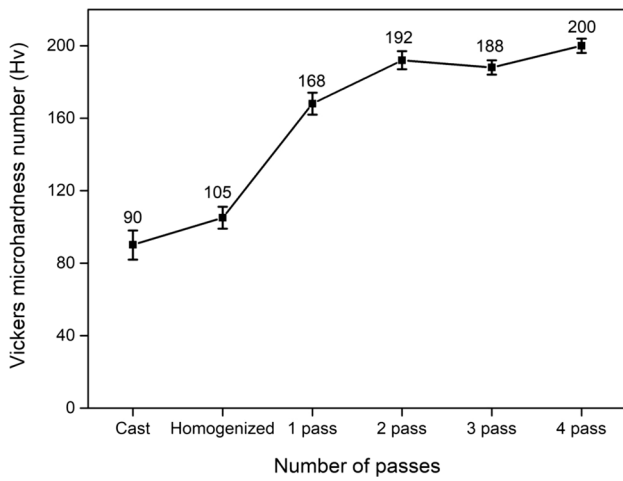
**Fig. 11** Microhardness of the alloy in different conditions



**Fig. 12** Engineering stress–strain diagram of the alloy in different conditions

third pass was decreased, it was 108% higher than the initial condition. Microhardness was enhanced by 122% after the fourth pass. The enhancement in the microhardness during the first and second passes is attributed to the decrease in the grain size of the material to submicrometer range, growth and evenly dispersion of finer precipitates in the material and work hardening of the material due to an increase in the dislocation density during ECAP processing (Ref 26). After the first pass, substantial enhancement in the hardness was perceived compared with later passes. Similar observation was perceived by Kim et al. (Ref 27) in 7075 Al alloy after ECAP processing. The decrease in the hardness of the material after the third pass is attributed to the reduction in the dislocation density of the material because dynamic recrystallization occurred during ECAP processing at high temperature (150 °C) and static recrystallization occurred due to preliminary heating of the specimen. Large amount of defect generated and accumulated during first two ECAP passes, must have promoted some amount of static recrystallization during preliminary heating done for the third pass. The decrease in the hardness of the material is also attributed to the texture modification occurring during ECAP processing. Hardness and strength of the material could be increased by decreasing the grain size if the texture is not much affected. Changes in the texture of the material could be observed from the variation in the intensities of the XRD peaks as shown in Fig. 10. It was perceived that cast and homogenized samples possess strong intensity of (111) peaks. In ECAP-processed samples, it was observed that the intensity of (111) peak was reduced. Also, intensity of (200) and (220) peaks was increased after ECAP processing. So it could be deduced that shear deformation happening during ECAP processing leads to a modification of the texture of the material. Chowdhury et al. (Ref 28) reported that deviation in the texture was observed in ECAP-processed Al alloy. Shaeri et al. (Ref 5) reported that maximum mechanical properties are achieved when the microstructure mainly consists of $\eta'$-phase precipitates in Al 7075 alloy. Xu et al. (Ref 21) reported that dissolution of the metastable $\eta'$ phase during ECAP processing at higher temperature leads to a decrease in mechanical properties of the Al 7034 cast alloy. Result in the present study is in consistent with the observations made in earlier reports from Shaeri et al. (Ref 5) and Xu et al. (Ref 21). From
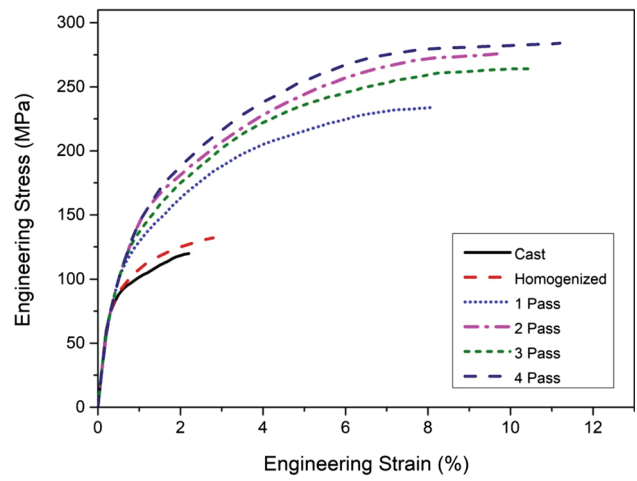
the TEM and XRD analysis, it is deduced that with an increase in the number of passes $\eta'$ phase transformed into $\eta$ phase. This may also be the reason for reduction in the hardness of the alloy after the third pass. It was reported that hardness was decreased after the third pass in ECAP-processed AZ31 magnesium alloy, and it is deduced that this is attributed to the softening of the material due to changes occurring in the texture of the material during ECAP processing (Ref 29). It was also reported that hardness was decreased after the third pass in ECAP-processed AM70 magnesium alloy, and it is deduced that this is attributed to the dynamic recrystallization occurring during ECAP at higher temperature and obstruction of the new grains to strain hardening (Ref 30).

**3.3.2 Strength and Ductility.** Figure 12 indicates the engineering stress–strain plots of the material in different conditions. It is noticed that cast and homogenized samples possess less strength and elongation to failure compared with ECAP-processed samples. Figure 13 indicates the UTS of the material in different conditions. In cast and homogenized conditions, the UTS of the material is $120 \pm 12$ and $132 \pm 12$ MPa, respectively. After ECAP processing, a substantial enhancement in the UTS of the material was observed. The UTS of the material was enhanced to $234 \pm 10$ and $276 \pm 10$ MPa in the first and second passes, respectively. But UTS was decreased to $264 \pm 6$ MPa in the third pass, and it again increased to $282 \pm 8$ MPa in the fourth pass. UTS was enhanced by 10% after homogenization treatment. After the first and second passes, the UTS was enhanced by 95 and 130%, respectively, from the initial condition. Even though the UTS of the alloy after third pass was decreased, it was still 120% higher than cast condition. UTS was enhanced by 135% after the fourth pass. The enhancement in the UTS of the material is attributed to the work hardening due to the interaction between the dislocations, Hall–Petch effect and precipitation strengthening (Ref 24). It is noted that after the third pass hardness was decreased. Hardness is interdependent on the strength of the material. Consequently, UTS of the material was also decreased after the third pass. A model was developed by Lukac and Balik to estimate the extent to which the softening and hardening mechanisms are possible during
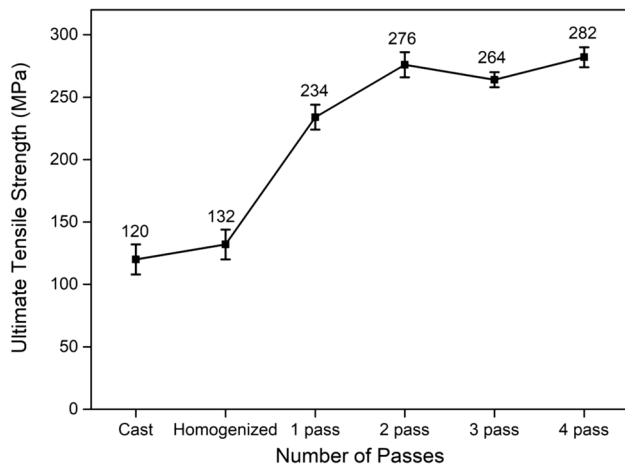
**Fig. 13** Ultimate tensile strength of the alloy in different conditions
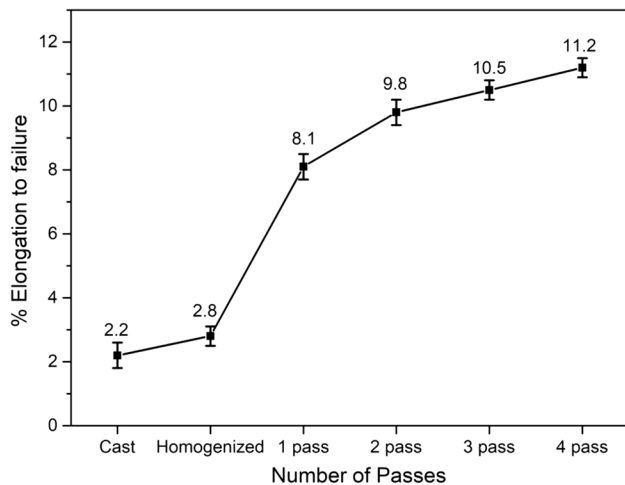


**Fig. 14** Elongation to failure of the alloy in different conditions

plastic forming of the materials. According to the model, the hardening happens if dislocation density increases due to the generation of forest dislocations and obstacles. In contrast, softening happens if dislocations migrate due to the dislocation climb and cross-slip (Ref 31).

Figure 14 presents the elongation to failure of the material in various stages. In cast and homogenized condition, the elongation to failure of the material is 2.2 ± 0.4 and 2.8 ± 0.3%, respectively. After ECAP processing, substantial enhancement in the elongation to failure of the material was perceived. The elongation to failure of the material was enhanced to 8.1 ± 0.4, 9.8 ± 0.4, 10.5 ± 0.3 and 11.2 ± 0.3% in the first pass, second pass, third pass and fourth pass, respectively. The cast and homogenized samples showed very poor ductility due to the presence of dendritic structure and defects such as microporosities (Ref 32). Pourbahari et al. (Ref 33) reported that, due to the presence of dendritic structure, volume defects such as inclusions and porosity lead to a decrease in the tensile strength and ductility of the AZ61 and GZ61 magnesium alloy. Enhancement in the elongation to failure after ECAP processing is attained due to the development of homogeneous and refined microstructure. Also, improvement in the ductility after ECAP processing is due to the reduction in cast defects (microporosities) (Ref 32).

It was perceived that, after ECAP processing along with enhancement in UTS of the material, elongation to failure was also enhanced, which is also a required property of engineering materials. This observation is in consistent with the earlier observations in cast Al-11Si alloy processed in rotary die ECAP (Ref 34) and cast Al-3Cu processed by ECAP (Ref 35). Enhancement in both strength and elongation to failure was also witnessed in Al-Zn-Mg alloys processed by ECAP up to four number of passes (Ref 36).

**3.3.3 Fractography.** Figure 15 presents the fracture modes of tensile test specimens and SEM images of the fracture surfaces of tensile test specimens in different conditions. It was noticed that fracture in the cast specimen occurred perpendicular to the major axis. The fracture mode perceived in the cast specimen is brittle fracture. Also, the fracture surface of the cast specimen was compiled with dendrites of size 20 μm and microporosities as shown in Fig. 15(a). Similar to cast specimen, fracture in the homogenized specimen occurred perpendicular to the major axis. The fracture mode perceived in the homogenized specimen is brittle fracture. But, the fracture surface was compiled of a few fairly large and deep dimples of size 5 μm, as presented in Fig. 15(b). Figure 15(c) shows the fracture mode of first-pass specimen. In this case, fracture has occurred approximately 45° to the major axis, and it was deduced that samples were failed in shear fracture mode. The change in fracture mode from brittle fracture to shear fracture is attributed to the strain hardening of the material during ECAP (Ref 37). The shear fracture mode was continued to appear in the second-, third- and fourth-pass samples as shown in Fig. 15(d), (e) and (f), respectively. After ECAP processing, a noticeable decrease in the size of the dimples was perceived. The dimple size is reduced to 2, 1, 0.7 and 0.4 μm in the first pass, second pass, third pass and fourth pass, respectively. Also after ECAP processing, shallower dimples were observed. The reduction in the dimple size is attained due to the refinement in the grain size during ECAP processing. The reduction in the dimple size with an increase in the ECAP passes is in consistent with earlier observations on ECAP-processed cast Al-Cu alloy (Ref 38), ECAP-processed Al-Zn alloy (Ref 39) and ECAP-processed AM70 magnesium alloy (Ref 30). The continuous reduction in the dimple size with an increase in the ECAP passes could be attributed to the grain refinement and the fragmentation of precipitates during ECAP processing (Ref 40).

## 4. Conclusions

In the present work, microstructural evolution and mechanical properties of the cast Al-5Zn-2Mg alloy processed by ECAP were studied. The Al-5Zn-2Mg alloy was successfully processed at 150 °C up to four number of passes. The major outcomes and conclusions of this work can be briefed as follows.

- After ECAP, a noticeable reduction in the grain size was identified. The dendrites size measured in the cast condition is 200 ± 20 μm, and after the fourth pass, the grain size is reduced to 3 ± 2 μm. In cast condition, rod-like $\eta'$-phase precipitates were observed, while after ECAP spherical-shaped $\eta$-phase precipitates were perceived and these precipitates were uniformly fragmented in the aluminum. After ECAP, high-density dislocations with high
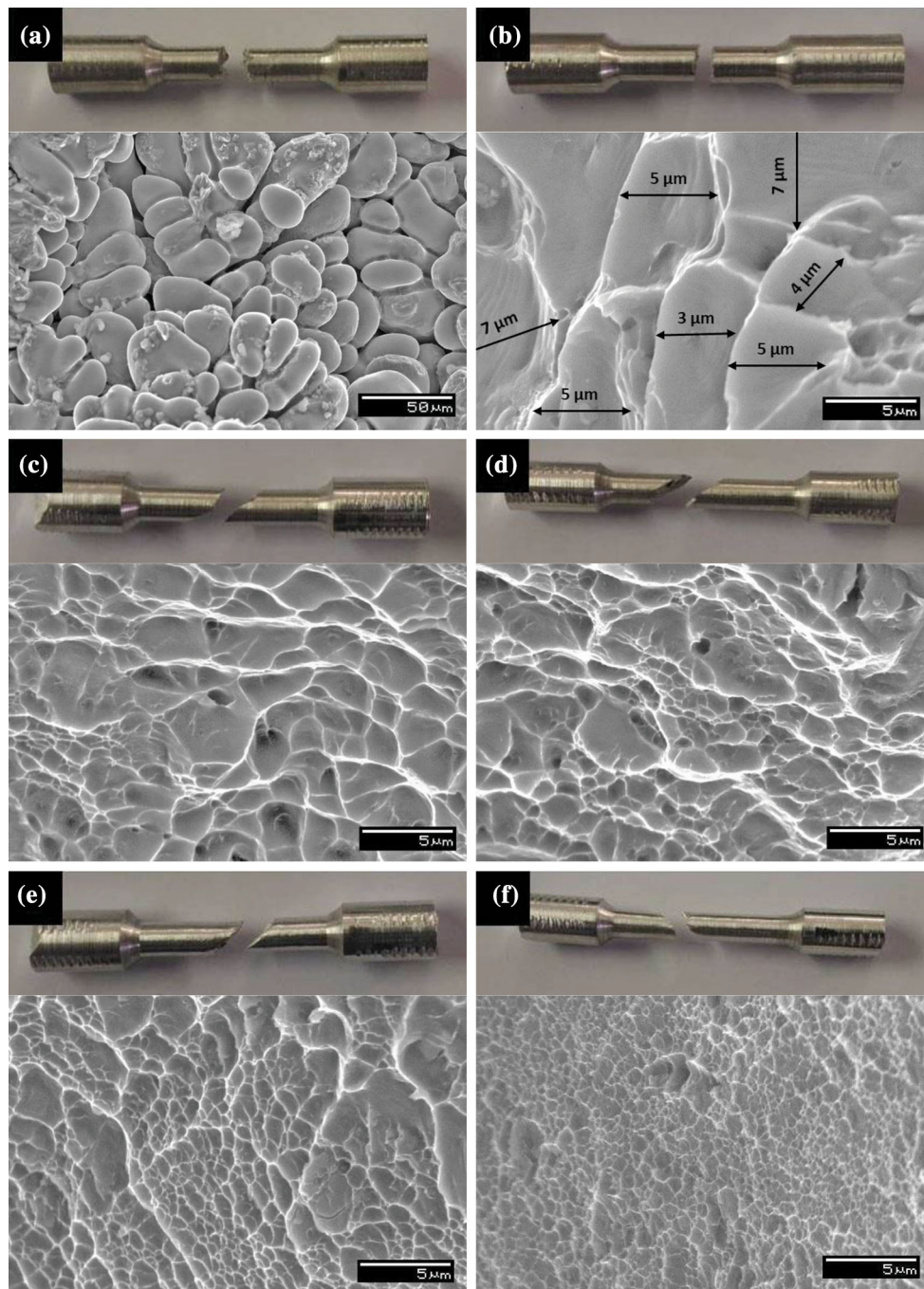
**Fig. 15** Fracture mode of the tensile test samples and SEM micrographs of the fracture surfaces of the tensile test samples (a) cast, (b) homogenized, (c) first pass, (d) second pass, (e) third pass and (f) fourth pass

angle of misorientation between the grains were perceived.

- After ECAP, a noticeable enhancement in the mechanical properties was identified. After four passes, the microhardness was enhanced to $200 \pm 4$ Hv (122% increase) and UTS was enhanced to $282 \pm 8$ MPa (135% increase) from the cast condition. Elongation to failure was enhanced from $2.2 \pm 0.4$ to $11.2 \pm 0.3$%. The enhancement in the mechanical properties is attained a decrease in the

grain size, homogenous microstructure, strain hardening, high dislocation density and finer precipitates homogenously distributed during ECAP processing.

- Brittle fracture mode was perceived in tensile testing of unprocessed specimens, while shear fracture mode was perceived in tensile testing of ECAP-processed specimens. Fracture surfaces of cast samples were composed of dendrites, while fracture surfaces of ECAP-processed samples were composed of dimples.

## References

1. R.Z. Valiev, R.K. Islamgaliev, and I.V. Alexandrov, Bulk Nanostructured Materials from Severe Plastic Deformation, *Prog. Mater. Sci.*, 2000, **45**(2), p 103–189

2. R.Z. Valiev and T.G. Langdon, Principles of Equal-Channel Angular Pressing as a Processing Tool for Grain Refinement, *Prog. Mater. Sci.*, 2006, **51**(7), p 881–981

3. V.M. Segal, V.I. Raznikov, A.E. Drobyshewsky, and V.I. Kopylov, Plastic Working of Metals by Simple Shear, *Russ. Metall.*, 1981, **1**, p 99–106

4. Y.T. Zehetbauer and M.J. Zhu, *Bulk Nanostrucutred Materials*, Wiley, Hoboken, 2009

5. M.H. Shaeri, M.T. Salehi, S.H. Seyyedein, M.R. Abutalebi, and J.K. Park, Microstructure and Mechanical Properties of Al-7075 Alloy Processed by Equal Channel Angular Pressing Combined with Aging Treatment, *Mater. Des.*, 2014, **57**, p 250–257

6. K. Gopala Krishna, K. Sivaprasad, T.S.N. Sankara Narayanan, and K.C. Hari Kumar, Localized Corrosion of an Ultrafine Grained Al-4Zn-2Mg Alloy Produced by Cryorolling, *Corros. Sci.*, 2012, **60**, p 82–89

7. K. Gopala Krishna, N. Singh, K. Venkateswarlu, and K.C. Hari Kumar, Tensile Behavior of Ultrafine-Grained Al-4Zn-2Mg Alloy Produced by Cryorolling, *J. Mater. Eng. Perform.*, 2011, **20**(9), p 1569–1574

8. A.A. Mazilkin, O.A. Kogtenkova, B.B. Straumal, R.Z. Valiev, and B. Baretzky, Formation of Nanostructure During High-Pressure Torsion of Al-Zn, Al-Mg and Al-Zn-Mg Alloys, *Defect Diffus. Forum*, 2005, **237–240**, p 739–744

9. O.A. Kogtenkova, A.A. Mazilkin, B.B. Straumal, G.E. Abrosimova, P. Zięba, T. Czeppe, B. Baretzky, and R.Z. Valiev, Phase Transformations in Al-Mg-Zn Alloys During High Pressure Torsion and Subsequent Heating, *J. Mater. Sci.*, 2013, **48**(13), p 4758–4765

10. A.A. Mazilkin, B. Baretzky, S. Enders, O.A. Kogtenkova, B.B. Straumal, E. Rabkin, and R.Z. Valiev, Hardness of Nanostructured Al-Zn, Al-Mg and Al-Zn-Mg Alloys Obtained by High-Pressure Torsion, *Defect Diffus. Forum*, 2006, **249**, p 155–160

11. K. Gopala Krishna, K. Sivaprasad, K. Venkateswarlu, and K.C. Hari Kumar, Microstructural Evolution and Aging Behavior of Cryorolled Al-4Zn-2Mg Alloy, *Mater. Sci. Eng. A*, 2012, **535**, p 129–135

12. S.L. Yang, Q.L. Lin, C. Xu, and J.H. Pan, Investigation on Fatigue Damage and Fracture of Al-5Zn-2Mg High Strength Aluminum Alloy, *Appl. Mech. Mater.*, 2012, **184–185**, p 1030–1033

13. Y. Iwahashi, J. Wang, Z. Horita, M. Nemoto, and T.G. Langdon, Principle of Equal-Channel Angular Pressing for the Processing of UltraFine Grained Materials, *Scr. Mater.*, 1996, **35**(2), p 143–146

14. K. Nakashima, Z. Horita, M. Nemoto, and T.G. Langdon, Development of a Multi-Pass Facility for Equal-Channel Angular Processing to High Total Strains, *Mater. Sci. Eng. A*, 2000, **281**(1–2), p 82–87

15. M. Furukawa, Z. Horita, and T.G. Langdon, Factors Influencing the Shearing Patterns in Equal-Channel Angular Pressing, *Mater. Sci. Eng. A*, 2002, **332**(1–2), p 97–109

16. O. Alvarez, C. Gonzalez, G. Aramburo, R. Herrera, and J.A. Juarez-islas, Characterization and Prediction of Microstructure in Al-Zn-Mg Alloys, *Mater. Sci. Eng. A*, 2005, **402**(1–2), p 320–324

17. S. Zhang, W. Hu, R. Berghammer, and G. Gottstein, Microstructure Evolution and Deformation Behavior of Ultrafine-Grained Al-Zn-Mg Alloys with Fine $\eta'$ Precipitates, *Acta Mater.*, 2010, **58**(20), p 6695–6705

18. K.R. Cardoso, D.N. Travessa, W.J. Botta, and A.M. Jorge, Jr., High Strength AA7050 Al Alloy Processed by ECAP: Microstructure and Mechanical Properties, *Mater. Sci. Eng. A*, 2011, **528**(18), p 5804–5811

19. S.D. Terhune, D. Swisher, K. Oh-Ishi, Z. Horita, T.G. Langdon, and T.R. McNelley, An Investigation of Microstructure and Grain-Boundary Evolution During ECA Pressing of Pure Aluminum, *Metall. Mater. Trans. A*, 2002, **33**(7), p 2173–2184

20. C. Xu, M. Furukawa, Z. Horita, and T.G. Langdon, Using ECAP to Achieve Grain Refinement, Precipitate Fragmentation and High Strain Rate Superplasticity in a Spray-Cast Aluminum Alloy, *Acta Mater.*, 2003, **51**(20), p 6139–6149

21. C. Xu, M. Furukawa, Z. Horita, and T.G. Langdon, Influence of ECAP on Precipitate Distributions in a Spray-Cast Aluminum Alloy, *Acta Mater.*, 2005, **53**(3), p 749–758

22. S.R. Kumar, K. Gudimetla, P. Venkatachalam, B. Ravisankar, and K. Jayasankar, Microstructural and Mechanical Properties of Al 7075 Alloy Processed by Equal Channel Angular Pressing, *Mater. Sci. Eng. A*, 2012, **533**, p 50–54

23. Y.H. Zhao, X.Z. Liao, Z. Jin, R.Z. Valiev, and Y.T. Zhu, Microstructures and Mechanical Properties of Ultrafine Grained 7075 Al Alloy Processed by ECAP and Their Evolutions During Annealing, *Acta Mater.*, 2004, **52**(15), p 4589–4599

24. J. Gubicza, I. Schiller, N.Q. Chinh, J. Illy, Z. Horita, and T.G. Langdon, The Effect of Severe Plastic Deformation on Precipitation in Supersaturated Al-Zn-Mg Alloys, *Mater. Sci. Eng. A*, 2007, **460–461**, p 77–85

25. M.H. Shaeri, M. Shaeri, M.T. Salehi, S.H. Seyyedein, and M.R. Abutalebi, Effect of Equal Channel Angular Pressing on Aging Treatment of Al-7075 Alloy, *Prog. Nat. Sci. Mater. Int.*, 2015, **25**(2), p 159–168

26. L.J. Zheng, H.X. Li, M.F. Hashmi, C.Q. Chen, Y. Zhang, and M.G. Zeng, Evolution of Microstructure and Strengthening of 7050 Al Alloy by ECAP Combined with Heat-Treatment, *J. Mater. Process. Technol.*, 2006, **171**(1), p 100–107

27. W.J. Kim, J.K. Kim, H.K. Kim, J.W. Park, and Y.H. Jeong, Effect of Post Equal-Channel-Angular-Pressing Aging on the Modified 7075 Al Alloy Containing Sc, *J. Alloys Compd.*, 2008, **450**(1–2), p 222–228

28. S.G. Chowdhury, C. Xu, and T.G. Langdon, Texture Evolution in an Aluminum Alloy Processed by ECAP with Concurrent Precipitate Fragmentation, *Mater. Sci. Eng. A*, 2008, **473**(1–2), p 219–225

29. A. Muralidhar, S. Narendranath, and H. Shivananda Nayaka, Effect of Equal Channel Angular Pressing on AZ31 Wrought Magnesium Alloys, *J. Magnes. Alloy.*, 2013, **1**(4), p 336–340

30. K.R. Gopi, H. Shivananda Nayaka, and S. Sahu, Investigation of Microstructure and Mechanical Properties of ECAP-Processed AM Series Magnesium Alloy, *J. Mater. Eng. Perform.*, 2016, **25**(9), p 3737–3745

31. P. Lukáč and J. Balík, Kinetics of Plastic Deformation, *Key Eng. Mater.*, 1994, **97–98**, p 307–322

32. G. Purcek, M. Aydin, O. Saray, and T. Kucukomeroglu, Enhancement of Tensile Ductility of Severe Plastically Deformed Two-Phase Zn-12Al Alloy by Equal Channel Angular Extrusion, *Mater. Sci. Forum*, 2009, **633–634**, p 437–447

33. B. Pourbahari, H. Mirzadeh, and M. Emamy, The Effects of Grain Refinement and Rare Earth Intermetallics on Mechanical Properties of As-Cast and Wrought Magnesium Alloys, *J. Mater. Eng. Perform.*, 2018, **27**(3), p 1327–1333

34. A. Ma, N. Saito, M. Takagi, Y. Nishida, H. Iwata, K. Suzuki, I. Shigematsu, and A. Watazu, Effect of Severe Plastic Deformation on Tensile Properties of a Cast Al-11 mass% Si Alloy, *Mater. Sci. Eng. A*, 2005, **395**(1–2), p 70–76

35. M.I.A. El Aal, Influence of the Pre-homogenization Treatment on the Microstructure Evolution and the Mechanical Properties of Al-Cu Alloys Processed by ECAP, *Mater. Sci. Eng. A*, 2011, **528**(22–23), p 6946–6957

36. Z.C. Duan, N.Q. Chinh, C. Xu, and T.G. Langdon, Developing Processing Routes for the Equal-Channel Angular Pressing of Age-Hardenable Aluminum Alloys, *Metall. Mater. Trans. A*, 2010, **41**(4), p 802–809

37. D.R. Fang, Q.Q. Duan, N.Q. Zhao, J.J. Li, S.D. Wu, and Z.F. Zhang, Tensile Properties and Fracture Mechanism of Al-Mg Alloy Subjected to Equal Channel Angular Pressing, *Mater. Sci. Eng. A*, 2007, **459**(1–2), p 137–144

38. M.I.A. El Aal, N. El Mahallawy, F.A. Shehata, M.A. El Hameed, E.Y. Yoon, J.H. Lee, and H.S. Kim, Tensile Properties and Fracture Characteristics of ECAP-Processed Al and Al-Cu Alloys, *Met. Mater. Int.*, 2010, **16**(5), p 709–716

39. O. Saray and G. Purcek, Microstructural Evolution and Mechanical Properties of Al-40 wt.% Zn Alloy Processed by Equal-Channel Angular Extrusion, *J. Mater. Process. Technol.*, 2009, **209**(5), p 2488–2498

40. A. Vinogradov, T. Ishida, K. Kitagawa, and V.I. Kopylov, Effect of Strain Path on Structure and Mechanical Behavior of Ultra-Fine Grain Cu-Cr Alloy Produced by Equal-Channel Angular Pressing, *Acta Mater.*, 2005, **53**(8), p 2181–2192